

## Positive-Definite and Monotonic Limiters for Unrestricted-Time-Step Transport Schemes

WILLIAM C. SKAMAROCK

*National Center for Atmospheric Research,\* Boulder, Colorado*

(Manuscript received 19 August 2005, in final form 19 October 2005)

### ABSTRACT

General positive-definite and monotonic limiters are described for use with unrestricted-Courant-number flux-form transport schemes. These limiters are tested using a time-split multidimensional transport scheme. The importance of minimizing the splitting errors associated with the time-split operator and of the consistency between the transport scheme and the discrete continuity equation is demonstrated.

### 1. Introduction

Scalar transport schemes in geophysical fluid flow models produce discrete solutions to the general scalar conservation equation

$$\frac{\partial \rho \phi}{\partial t} + \nabla \cdot \rho \mathbf{V} \phi = 0, \quad (1a)$$

where  $\phi$  is a scalar mixing ratio,  $\rho$  is the air density,  $\mathbf{V}$  is a velocity vector, and the operator  $\nabla \cdot$  represents a multidimensional flux divergence. Additionally, the mass fluxes  $\rho \mathbf{V}$  satisfy the mass conservation equation

$$\frac{\partial \rho}{\partial t} + \nabla \cdot \rho \mathbf{V} = 0. \quad (1b)$$

Discrete solvers for the scalar transport equation appear in a number of important geophysical fluid dynamics applications, including climate, weather, and ocean modeling, and air quality and air chemistry modeling. Typically these solvers are based on extensions of schemes developed for one-dimensional transport—for which a wide variety of schemes have been developed.

Relative to the large number of one-dimensional schemes described in the literature, there are many

fewer multidimensional schemes because of the additional complexities that arise in attempting to extend the 1D schemes while simultaneously preserving valuable scheme properties such as monotonicity and conservation. Existing multidimensional transport schemes can be grouped into two general categories. First, 3D schemes can be constructed in a fully explicit manner where all the cross terms are explicitly derived and represented in the algorithm and resulting code. Examples of this approach can be found in Leveque (1996), Leonard et al. (1996, hereafter referred to as LLM96), and Stevens and Bretherton (1996). Second, algorithms for 3D transport have been constructed based on sequential application of 1D schemes. These algorithms are called *time split*, and examples of this type of splitting include Easter (1993), Walcek (2000), and Clappier (1998).

Recently, so-called unrestricted-time-step schemes have been implemented in large-scale Eulerian models (e.g., LLM96; Lin and Rood 1996, hereafter referred to as LR96). These schemes are based on 1D schemes and they can be cast in both time-split and nonsplit forms (LLM96). In both LLM96 and LR96 it is found that the positive-definite and monotonic limiters used with their transport schemes are no longer absolutely positive-definite or monotonic (to machine roundoff) for Courant numbers  $|U\Delta t/\Delta x| > 1$ . We have verified this behavior of the limiters in the unrestricted-time-step schemes and we have designed two new general limiters that are positive-definite and monotonic (to machine roundoff). In this paper, we describe the limiter formulations and test them in 2D and 3D applications using a

\* The National Center for Atmospheric Research is sponsored by the National Science Foundation.

*Corresponding author address:* William C. Skamarock, National Center for Atmospheric Research, P.O. Box 3000, Boulder, CO 80307-3000.  
E-mail: skamaroc@ucar.edu

time-split solver based on the LLM96 scheme that models the transport of a scalar in a compressible fluid. We highlight the importance of minimizing the splitting errors associated with the time-split operator, and the need for consistency between the transport scheme and the discrete continuity equation is also demonstrated. Given that the fully explicit schemes of LLM96 and LR96 have costs that scale approximately as  $n^2$  ( $n$  is the number of spatial dimensions) whereas the cost of time-split schemes scale approximately as  $n$ , the time-split formulations offer attractive and cost-effective alternatives to LLM96 and LR96 for some applications.

## 2. Unrestricted-time-step time-split transport scheme

### a. Basic time-split scheme

A one-dimensional forward-in-time (FIT) discretization of (1a) and (1b) can be written as

$$(\rho\phi)^{t+\Delta t} = (\rho\phi)^t - F_x(\phi^t), \quad (2a)$$

$$\rho^{t+\Delta t} = \rho^t - F_x(I), \quad (2b)$$

where superscripts denote the solution time level and the vector  $I \equiv 1$ . The operator  $F_x$  denotes the discrete flux divergence in  $x$  and is typically expressed as

$$F_x(\phi) = (\Delta t/\Delta x)[f(\phi)_{x+\Delta x/2} - f(\phi)_{x-\Delta x/2}].$$

To construct the fluxes  $f$ , the mass fluxes at the faces  $(\rho u)_{x\pm\Delta x/2}$  are multiplied with values of  $\phi_{x\pm\Delta x/2}$  that are determined through some form of interpolation or integration (i.e., the advection scheme). The mass fluxes  $(\rho u)_{x\pm\Delta x/2}$  are identical to those used in the mass conservation Eq. (2b).

The mass conservation Eq. (1b) is usually solved within a full dynamical model and is discretized within a 3D formulation as

$$\rho^{t+\Delta t} = \rho^t - F_x(I) - F_y(I) - F_z(I). \quad (3)$$

To extend the 1D scalar scheme (2a) to multiple dimensions, we follow the formulation of Easter (1993) wherein the mass conservation Eq. (3) is simultaneously reintegrated with the discrete version of the continuous transport Eq. (2a). The 3D algorithm is

$$(\rho\phi)^* = (\rho\phi)^t - F_x(\phi^t), \quad (4a)$$

$$\rho^* = \rho^t - F_x(I), \quad (4b)$$

$$\phi^* = (\rho\phi)^*/(\rho)^*, \quad (4c)$$

$$(\rho\phi)^{**} = (\rho\phi)^* - F_y(\phi^*), \quad (4d)$$

$$\rho^{**} = \rho^* - F_y(I), \quad (4e)$$

$$\phi^{**} = (\rho\phi)^{**}/(\rho)^{**}, \quad (4f)$$

$$(\rho\phi)^{t+\Delta t} = (\rho\phi)^{**} - F_z(\phi^{**}), \quad (4g)$$

$$\rho^{t+\Delta t} = \rho^{**} - F_z(I), \quad (4h)$$

$$\phi^{t+\Delta t} = (\rho\phi)^{t+\Delta t}/\rho^{t+\Delta t}. \quad (4i)$$

It can easily be seen that the scheme (4) collapses to (3) for  $\phi = I$ , and hence is consistent (i.e., if  $\phi = \text{constant}$  at the initial time, it remains constant for all time; see LR96 for further discussion). Additionally, the time-split scheme (4) is only first-order accurate in time. A form of Strang splitting (Strang 1968) can be used to achieve second-order accuracy. Strang splitting for (4) consists of alternating the order of the splitting each time step; the order of the flux divergence operators is alternated between  $x \rightarrow y \rightarrow z$  as in (4) and  $z \rightarrow y \rightarrow x$  (see LLM96 for a 2D example).

Figure 1 shows results for a 2D test problem, described in the appendix, for the advection of a passive tracer in a deformational flow field (Durrant 1999, section 5.7.4). Results from a 2D solver using the piecewise parabolic method (PPM; Carpenter et al. 1990) and Eq. (4) with Strang splitting are compared with results from the COSMIC (LLM96) solver. The comparison indicates that both solvers produce very similar solutions using  $\Delta x = 0.02$ . The PPM solution for  $\Delta x = 0.01$  is also shown to demonstrate that the solutions converge (the COSMIC solution at  $\Delta x = 0.01$  is almost identical). The PPM time-split solver has slightly more than half as many operations as the 2D explicit COSMIC solver but a similar level of accuracy as measured in the  $L_2$  and  $L_\infty$  norms. Thus the PPM solver is significantly more efficient for this level of accuracy.

Figure 2 depicts the results for three permutations of the PPM solver we have described. Figure 2a shows the PPM solution that does not use Strang splitting ( $x \rightarrow y$  each time step) and that is mass inconsistent ( $\rho^t$  is used in each substep to recover the mixing ratio). Figure 2b depicts the results using Strang splitting ( $x \rightarrow y$  followed by  $y \rightarrow x$ ) but is still mass inconsistent. Figure 2c depicts a mass-consistent result [using (4)] without using Strang splitting. It is obvious in these results that both mass consistency and second-order-accurate splitting are important for optimizing scheme accuracy.

### b. Removing the Courant number restriction

Most of the one-dimensional FIT schemes described in the literature have a Courant number limitation  $|\text{Cr}| = |U\Delta t/\Delta x| \leq 1$ , and extensions of these schemes to multiple dimensions usually result in a Courant number limit  $|\text{Cr}_x|, |\text{Cr}_y| \leq 1$  as opposed to the more restrictive condition  $|\text{Cr}_x| + |\text{Cr}_y| \leq 1$ . For applications where the

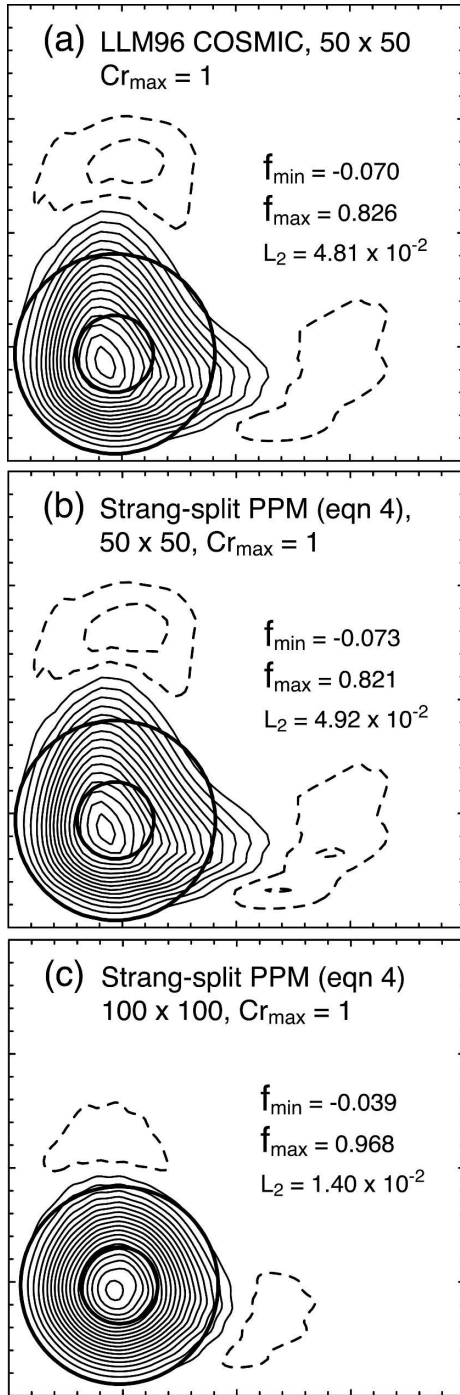


FIG. 1. Comparison of exact solution with numerical solutions for the 2D test problem described in the appendix. The thick lines are the 0.05 and 0.75 contours for the exact solution. The numerical solutions are contoured with a contour interval of 0.05 beginning at 0.05, and the dashed contours are  $-0.01$  and  $-0.05$ . The plotted domain is  $(0:1, 0:1)$  and the number of grid cells are given for each plot, as is the maximum Courant number for the simulation, the maximum and minimum in the numerical solution, and the  $L_2$  error norm. The maximum/minimum for the exact solution is  $1/0$ .

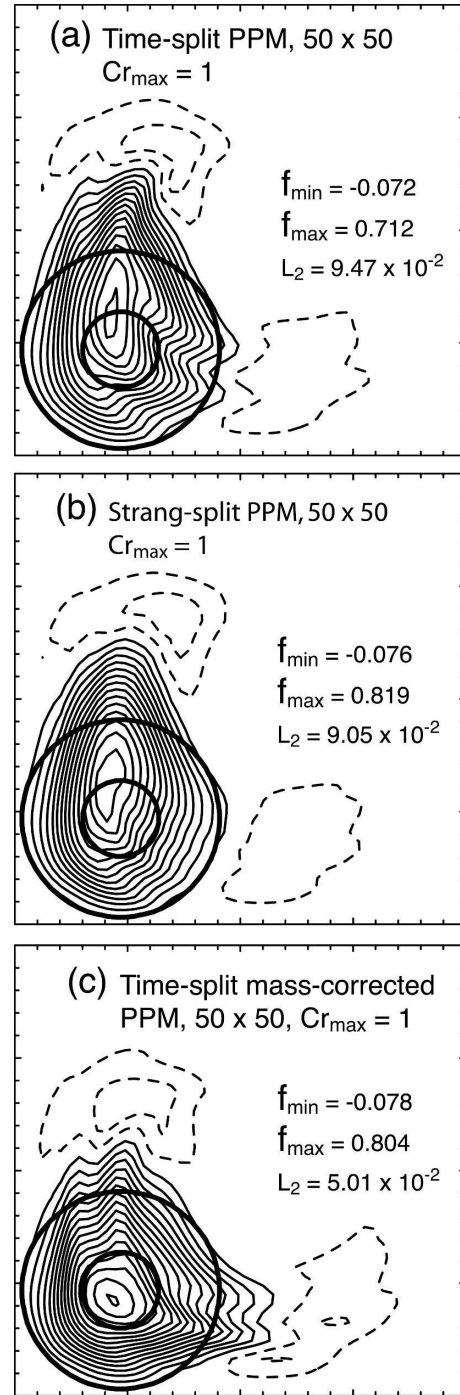


FIG. 2. (a) Time-split PPM solution without mass correction or Strang splitting. (b) Strang-split PPM without mass correction. (c) Mass-corrected PPM without Strang splitting. Plotted as in Fig. 1.

flow field is well resolved it may be advantageous to use a time step dictated by accuracy as opposed to one limited by a Courant number.

Two general approaches have been developed to remove the Courant number restriction. Semi-

Lagrangian schemes are limited by the Lipschitz number  $\Delta t |(\partial u / \partial x)| < 1$  as opposed to the Courant number. The schemes are based on the characteristic (advective form) equations, where fluid trajectories are calculated and mixing-ratio values are interpolated from the regular grid points to the trajectory departure points (when using *backward* trajectories), or from the arrival points to the regular grid points (when using *forward* trajectories) in the updating process [see Staniforth and Cote (1991) for a complete review]. The advective form of the transport equation does not naturally lead to schemes that are locally or globally conservative, although formulations exist that possess local and/or global conservation, for example, Bermejo and Conde (2002), Nair and Machenhauer (2002), and Leslie and Purser (1995).

In an alternative approach using the conservation form of the governing equations, LR96 presents a modification to the one-dimensional flux calculation that removes the Courant number restriction for any FIT scheme that is limited by  $|\text{Cr}| \leq 1$ . Our implementation of this scheme begins with the discrete form of the mass conservation Eq. (1a) in one spatial dimension:

$$\rho_i^{t+\Delta t} = \rho_i^t - \Delta t \delta_x [(\tilde{\rho}u)_{i+1/2} - (\tilde{\rho}u)_{i-1/2}].$$

The discrete index  $i$  maps to physical space  $x = i\Delta x$ . Following the standard discretization approach, the mass fluxes  $\Delta t \tilde{\rho}u$  are specified at the control volume faces at  $i \pm 1/2$ . In the LR96 formulation, these mass fluxes are decomposed into integer (or full) and fractional fluxes as follows:

$$\begin{aligned} \Delta t (\tilde{\rho}u)_{i-1/2} &= \sum_{k=1}^{K_{i-1/2}} (\rho^t \Delta x)_{i-k} + \text{Cr}'_{i-1/2} (\rho^t \Delta x)_{i-1-K_{i-1/2}}, \\ &\tilde{\rho}u > 0 \\ &= \sum_{k=1}^{K_{i-1/2}} -(\rho^t \Delta x)_{i-1+k} + \text{Cr}'_{i-1/2} (\rho^t \Delta x)_{i+K_{i-1/2}}, \\ &\tilde{\rho}u < 0. \end{aligned} \quad (5)$$

The integer Courant numbers at the control volume faces  $K_{i-1/2}$  and the fractional Courant numbers ( $\text{Cr}'_{i-1/2}$ ) are determined by (5). Note that the integer Courant number  $K$  is defined as positive here, even for negative fluxes. The fractional Courant number  $\text{Cr}'_{i-1/2}$  is computed by increasing  $K$  until  $(0 \leq \text{Cr}'_{i-1/2} < 1)$  for  $\tilde{\rho}u > 0$  or  $(-1 < \text{Cr}'_{i-1/2} \leq 0)$  for  $\tilde{\rho}u < 0$ .

To advance the discrete form of the scalar conservation Eq. (1a)

$$(\rho\phi)_i^{t+\Delta t} = (\rho\phi)_i^t - \Delta t \delta_x [f(\phi')_{i+1/2} - f(\phi')_{i-1/2}],$$

the scalar fluxes  $f(\phi')_{i-1/2}$  are specified as

$$\begin{aligned} \Delta t f(\phi')_{i-1/2} &= \sum_{k=1}^{K_{i-1/2}} (\rho\phi\Delta x)_{i-k}^t \\ &+ f'(\phi', \text{Cr}'_{i-1/2}, i-1/2 - K_{i-1/2}), \\ &\tilde{\rho}u > 0 \\ &= \sum_{k=1}^{K_{i+1/2}} -(\rho\phi\Delta x)_{i+k-1}^t \\ &+ f'(\phi', \text{Cr}'_{i-1/2}, i-1/2 + K_{i+1/2}), \\ &\tilde{\rho}u < 0. \end{aligned} \quad (6)$$

The fractional fluxes and  $f'(\phi')_{i-1/2}$  are computed using the base advection scheme evaluated at the appropriately shifted control-volume face,  $i - 1/2 - K_{i-1/2}$  for  $\tilde{\rho}u > 0$  and  $i - 1/2 + K_{i-1/2}$  for  $\tilde{\rho}u < 0$ , and using the fractional Courant number  $\text{Cr}'_{i-1/2}$ .

LR96 and LLM96 use this approach within their non-time-split schemes to remove the Courant number limitations of their base advection schemes. This approach also works well in the time-split scheme (4) using Strang splitting. Figure 3 depicts results using time steps that have maximum Courant numbers 4 times larger than the results shown in Fig. 1. The results show that the errors are similar at both time steps;  $\phi_{\text{max}}$  is slightly reduced in the large time step simulation but the  $L_2$  error is unchanged. The two different schemes (split PPM and COSMIC) work well at Courant numbers much larger than 1. The additional cost incurred in using (5) and (6) is small relative to the advection operators (PPM in this case). Thus the similarity of the results produced by the extended scheme (6) and COSMIC indicates that the scheme (6) is significantly more efficient for this problem. In addition, the splitting errors in the extended scheme have not become more noticeable with the larger time step.

As in semi-Lagrangian schemes, the Courant-number-unlimited scheme we have outlined has time step restrictions based the Lipschitz number  $\Delta t |(\partial u / \partial x)| < 1$ . In semi-Lagrangian schemes this restriction can be understood as restricting trajectories such that they do not intersect (Smolarkiewicz and Pudykiewicz 1992). For the flux formulation (5) and (6), the restriction can be understood as not allowing mass to be completely evacuated from a grid cell in a single 1D substep in (4), which would be the practical result of intersecting trajectories.

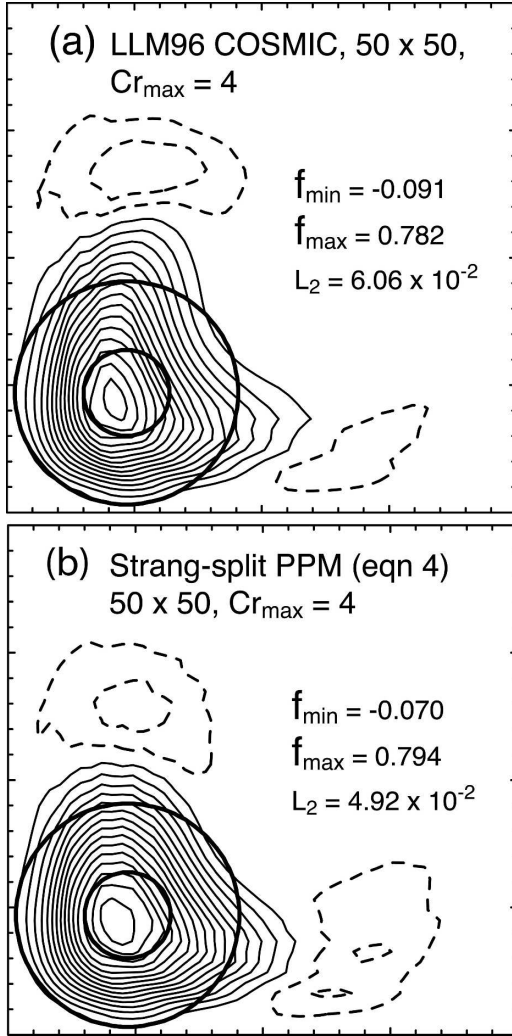


FIG. 3. (a) COSMIC and (b) PMM results for large Courant numbers ( $Cr_{\max} = 4$ ) using the unrestricted-time-step formulations. Plotted as in Fig. 1.

### 3. Positive-definite and monotonic limiters

#### a. Formulation of the limiters

A scheme is *positive definite* if it does not generate negative mixing ratios  $\phi$  from nonnegative initial mixing ratios. Following Thuburn (1996), a scheme is *monotonic*<sup>1</sup> if it does not amplify extrema in the initial mixing ratios. A monotonic scheme is positive definite and is also consistent (a constant mixing ratio will remain constant; see LR96). A number of techniques exist for rendering conservative flux-form FIT schemes either positive definite or monotonic. Typically schemes modify or limit the fluxes to achieve monoto-

nicity or positive definiteness, or they will modify the value of the mixing ratio  $\phi$  that multiplies the mass flux on a cell face from which the flux divergence is calculated.

As noted in the introduction, positive-definite or monotonic limiters typically used with the base advection schemes are no longer absolutely positive definite or monotonic in the unrestricted-time-step formulations of LR96 and LLM96. We have examined two limiters for use with the time-split scheme (4) and the Courant-number-unlimited flux evaluations (6). For positive-definite transport, the renormalization approach described in Smolarkiewicz (1989) can be extended to applications with  $|Cr| > 1$ . The base ( $|Cr| \leq 1$ ) Smolarkiewicz (1989) algorithm begins with a calculation of the full fluxes. Next, a lower bound on the full update is determined by computing the flux divergence for each cell using only the outgoing fluxes,

$$(\rho\phi)^* = (\rho\phi)^t - \Delta t \sum_{i=1}^n \delta_{x_i} [f_i]^+, \quad (7)$$

where  $(\rho\phi)^*$  is the lower bound on the update and  $[f_i]^+$  denotes the outgoing fluxes in the  $i$  coordinate direction ( $x, y, z$ ). Note that the incoming fluxes are not considered in the renormalization—they can only act to increase the mixing ratio, not decrease it; thus  $(\rho\phi)^*$  is a lower bound. If this lower bound is less than zero, the outgoing fluxes are renormalized by multiplication with a constant such that the lower bound becomes zero:

$$f_j^{+*} = f_j^+ (\rho\phi)^t \left( \Delta t \sum_{i=1}^n \delta_{x_i} [f_i]^+ \right)^{-1}. \quad (8)$$

We have found it necessary to modify (7) and (8) for use with the Courant-number-unlimited scheme. First, we recast the fractional flux associated with the fractional Courant number  $Cr'$  [see (5) and (6)] as the sum of the first-order upwind flux plus a remaining higher-order correction. Second, we calculate a partial update of the scalar mass in the cell using both the integer fluxes and the fractional first-order upwind fluxes. This update is positive definite and monotonic—it is the first-order upwind solution. Finally, we apply the renormalization steps (7) and (8) to the remaining higher-order corrective fluxes using the computed partial update in place of  $(\rho\phi)^t$ . Results for the 2D test case are shown in Figs. 4a and 4b. Negative mixing ratios are eliminated using this procedure. Comparison with the non-positive-definite solutions (Figs. 1b and 2b) shows that solution accuracy is maintained in this test case; solution errors are similar for the tests at the two Courant numbers.

<sup>1</sup> Thuburn (1996) uses the term *shape preserving*.

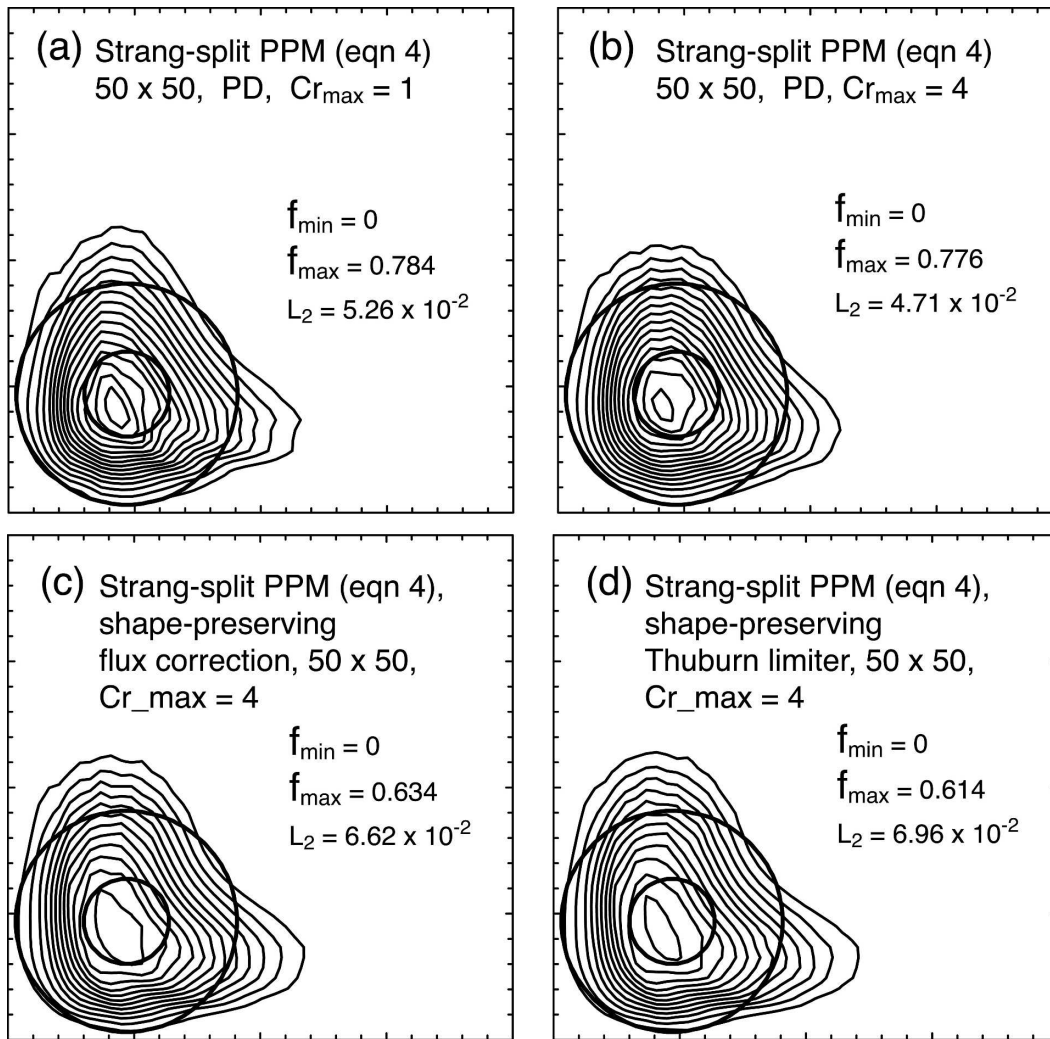


FIG. 4. Results for the positive-definite limiter for Courant numbers (a)  $Cr_{max} = 1$  and (b)  $Cr_{max} = 4$ . Monotonic test results for  $Cr_{max} = 4$  using (c) flux renormalization and (d) the modified Thuburn limiter. Plotted as in Fig. 1.

For monotonicity, we have examined an extension of the Smolarkiewicz (1989) renormalization approach mentioned in Durran (1999) and the universal limiter described in Thuburn (1996) originally developed for 1D applications as described in Leonard (1991). The renormalization approach is extended by using nonzero upper and nonzero lower bounds,  $(\rho^{t+\Delta t}\phi_{min,max})$ , on  $\phi^*$  in (7). Here  $\phi_{min,max}$  are the minimum and maximum values of  $\phi^t$  sampled from the updated cell and all cells that contribute to the flux divergence calculation in (6). Additionally, the renormalization (8) is replaced by

$$f_j^{\pm*} = f_j^{\pm} |(\rho\phi)^t - (\rho^{t+\Delta t}\phi_{min,max})| \left( \Delta t \sum_{i=1}^n \delta_{x_i} [f_i]^{\pm} \right)^{-1}. \quad (9)$$

The positive option in (9) is for the lower bound and the negative option is for the upper bound, and  $f_i^{\pm}$  are incoming and outgoing fluxes, respectively. Results for this monotonic renormalization for the 2D test problem are given in Fig. 4c. The results are similar to that produced with the positive-definite limiter (Fig. 4b) except that the solutions are slightly more diffuse and the solution peak values are more damped. The  $L_2$  errors have also increased because of the increased damping in the monotonic renormalization.

Thuburn (1996) presents an algorithm for a universal multidimensional monotonic limiter, and we have adapted this limiter for the 1D version of our time-split transport scheme (4) and the Courant-number-unlimited extension (6). The Thuburn limiter uses upwind-based bounds, and we use lower and upper

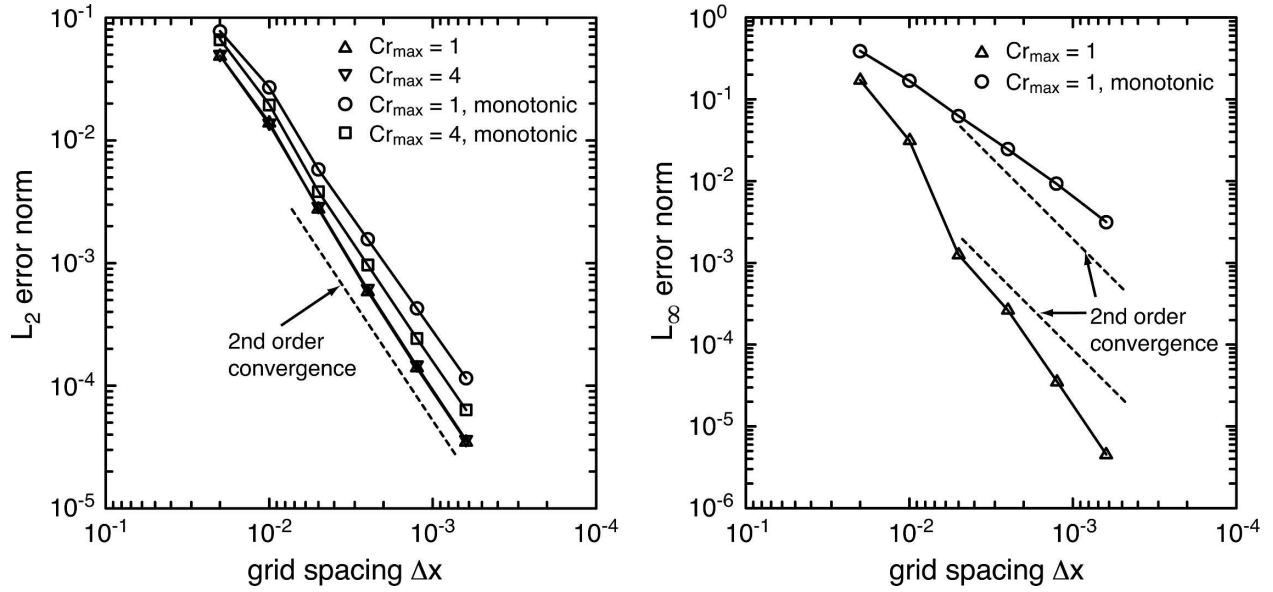


FIG. 5. Convergence rates in the (left)  $L_2$  and (right)  $L_\infty$  norms for the 2D test problem. Monotonic flux renormalization is used where noted.

bounds determined upwind relative to the fractional flux faces for extension to the Courant-number-unlimited scheme. In our tests we find that the resulting transport scheme is no longer monotonic, rather small overshoots and undershoots are produced. This behavior is similar to the findings in LLM96 who used a different scheme and limiter; because of the generation of very small over- and undershoots they called their scheme *essentially monotonic*. LR96 also note that their version of PPM, using the standard PPM limiters (see the appendix in LR96), is no longer exactly monotonic for Courant numbers greater than 1.

Examination of the Thuburn limiting process reveals that monotonicity can be lost when the integer flux counts  $K$  differ on two successive cell faces in our 1D application. We have found that monotonicity can be restored if two additional constraints are applied. First, in Thuburn's computation of the computed minimum and maximum outwardly fluxed mixing ratios for cell  $k$  (using Thuburn's notation), we bound  $(\hat{q}_k^{(out)})_{max}$  [Eq. (43) in Thuburn (1996)] by  $(\hat{q}_i^{(in)})_{min}$  (the minimum of the cell value and all fractional upwind flux components), and we bound  $(\hat{q}_k^{(out)})_{min}$  [Eq. (44) in Thuburn (1996)] by  $(\hat{q}_i^{(in)})_{max}$  (the maximum of the cell value and all fractional upwind flux components). Additionally, if this bounded maximum outwardly fluxed mixing ratio for cell  $k$ ,  $(\hat{q}_k^{(out)})_{max}$ , is less than the bounded minimum,  $(\hat{q}_k^{(out)})_{min}$ , the limits are erroneous because of the integer fluxes and we replace the flux-face values for the  $k$ th cell face by their upwind values [i.e., we use

upwind values  $\hat{q}_i, \hat{q}_j$  in Thuburn's scalar update Eq. (9) for the fluxes associated with this cell].

Results for the 2D test problem using this limiter with the time-split scheme (4) and the Courant number extension (6) are shown in Fig. 4d. The results are not identical to those using renormalization, but they are very similar; the solution peak is slightly more damped at  $Cr_{max} = 4$  compared with the monotonic renormalization scheme.

#### b. Convergence tests

A comparison of results using the Thuburn monotonic limiter (Fig. 4d) with results from the positive-definite limiter (Fig. 4b) illustrates the increased damping generally associated with monotonicity. For smooth solutions such as those for our 2D test problem, monotonic schemes can degrade the solution accuracy relative to solutions produced by other schemes. The degraded solution accuracy is quantified in Fig. 5, which depicts the  $L_2$  and  $L_\infty$  error norms for the 2D test problem using different space and time steps for the non-monotonic and monotonic schemes. For the  $L_2$  error norm,

$$L_2 = \left\{ \sum_{i=1}^N [\phi_{\text{exact}} - \phi(i)]/N \right\}^{1/2},$$

where  $N$  is the number of grid points, there is a noticeable drop in solution accuracy using the monotonic scheme although the convergence rate remains almost

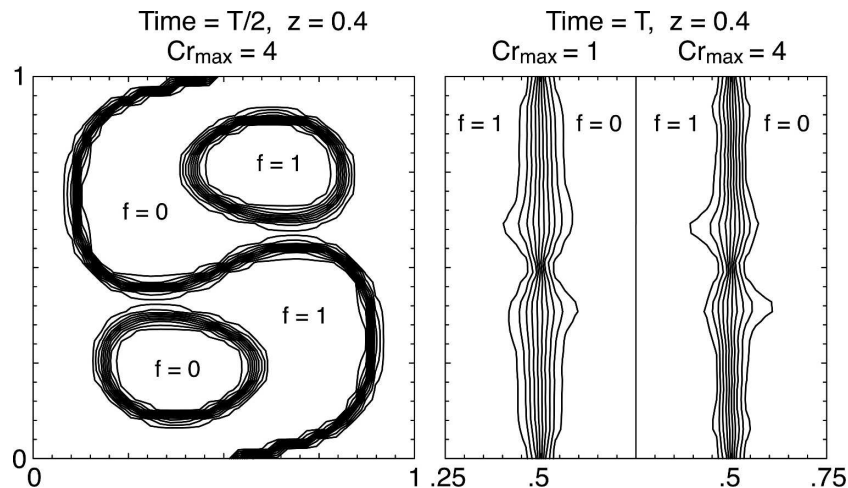


FIG. 6. Three-dimensional test results using Strang-split mass-corrected PPM scheme with the Thuburn monotonic limiter. The contour interval is 0.1 beginning at 0.05. These results should be compared with Leveque (1996, Fig. 11.2).

second order. The  $L_\infty$  norm (the absolute value of the maximum error) shows a more dramatic drop in solution accuracy and in the convergence rate when using the monotonic scheme. The  $L_2$  error-norm results illustrate the overall second-order accuracy of the time-split scheme. The nonmonotonic results using Courant numbers of 1 and 4 produce  $L_2$  error norms that are almost indistinguishable, suggesting that the time-truncation error is small for this scheme and test problem configuration.

### c. Three-dimensional test with a discontinuity

Monotonic schemes tend to damp more, are less accurate, and are more expensive than their nonmonotonic counterparts, and for these reasons they are not used in many applications. Monotonic schemes are most often used for problems where sharp discontinuities exist in the solutions; nonmonotonic schemes may produce undesirable nonphysical over- and undershoots in the vicinity of the discontinuities.

To further test the schemes we use the 3D test problem described in Leveque (1996) that is outlined in the appendix. This test features a strong deformational flow and a discontinuity that is advected by the 3D flow field. Results for the test problem are given in Fig. 6. The time-split scheme produces similar results for maximum Courant numbers of 1 and 4. The  $Cr_{\max} = 4$  solution even appears to be slightly less diffuse at the end time, likely because the  $Cr_{\max} = 1$  solution has effectively 4 times as many limiter applications given it needs 4 times as many time steps than the  $Cr_{\max} = 4$  solution to reach the end time. Not shown are results

from the renormalization-based monotonic scheme; the results are almost identical to those from the Thuburn-based limiter at both maximum Courant numbers of 1 and 4. The present results are also very similar to the results given by Leveque (1996, section 11.2, Fig. 11.2) that were computed with a fully 3D scheme using  $Cr_{\max} = 1$ . The limiter used by Leveque does not guarantee monotonicity—small over- and undershoots are present in his solution.

## 4. Summary

We have developed formulations for universal limiters that are positive definite or monotonic that work for unrestricted-time-step schemes. Specifically:

- 1) Positive-definite limiters using renormalization (following Smolarkiewicz 1989) can be extended for use with Courant-number-unlimited formulations. The positive-definite limiter retains exact positive-definite behavior (to machine roundoff).
- 2) Monotonic limiters using renormalization [Durrant (1999) extension of Smolarkiewicz (1989)] and a Thuburn (1996) monotonic limiter can be applied to the Courant-number-unlimited schemes with minor modifications. Monotonicity is exact (to machine roundoff).

Our motivation for examining time-split multidimensional transport schemes is the recognition of the high computational cost of unsplit schemes (compared to split schemes) for 3D transport along with the difficulty encountered formulating positive-definite and mono-

tonic versions of the fully multidimensional schemes. The latter difficulties are exacerbated when schemes are extended to Courant-number-unlimited formulations such as LR96 and LLM96. The positive-definite and monotonic renormalizations that we have tested can be used with fully multidimensional schemes (such as those in LR96 and LLM96). The renormalization Eqs. (8) and (9) (for positive-definite and monotonic applications, respectively) are valid for transport problems of any dimensionality. Additional effort may be needed to identify the appropriate bounds  $\phi_{\min, \max}$  in multidimensional applications and in Courant-number-unlimited formulations such as LR96 and LLM96.

## APPENDIX

### Test Cases and PPM Scheme

#### a. Two-dimensional test problem

A two-dimensional test problem for advection of a passive tracer in a nondivergent deformational flow field is presented in Durran (1999, section 5.7.4). The computational domain is the unit square ( $0 \leq x \leq 1$ ;  $0 \leq y \leq 1$ ) and the initial mixing ratio is

$$\phi(x, y, t = 0) = \frac{1}{2}[1 + \cos(\pi r)],$$

where

$$r(x, y) = \min\left\{1, 4\left[\left(x - \frac{1}{4}\right)^2 + \left(y - \frac{1}{4}\right)^2\right]^{1/2}\right\}.$$

The velocity fields are given by

$$u(x, y, t) = \sin^2(\pi x) \sin(2\pi y) \cos(\pi t/5)$$

$$v(x, y, t) = -\sin^2(\pi y) \sin(2\pi x) \cos(\pi t/5).$$

The velocity fields, initial condition, and solution at time  $t = 2.5$  is given in Fig. A1. The velocity fields are such that the tracer field evolves from the initial smooth state to the highly deformed state (at  $t = 2.5$ ) and then back to the initial state at time  $t = 5$ . Further details are given in Durran (1999).

#### b. Three-dimensional test problem

A three-dimensional test problem for scalar transport in a nondivergent deformational flow field is presented in Leveque (1996, section 11, example 11.2) for the unit cube. The test problem is designed in a manner similar to the previous 2D test problem in Durran (1999) in that the velocity fields are constructed such

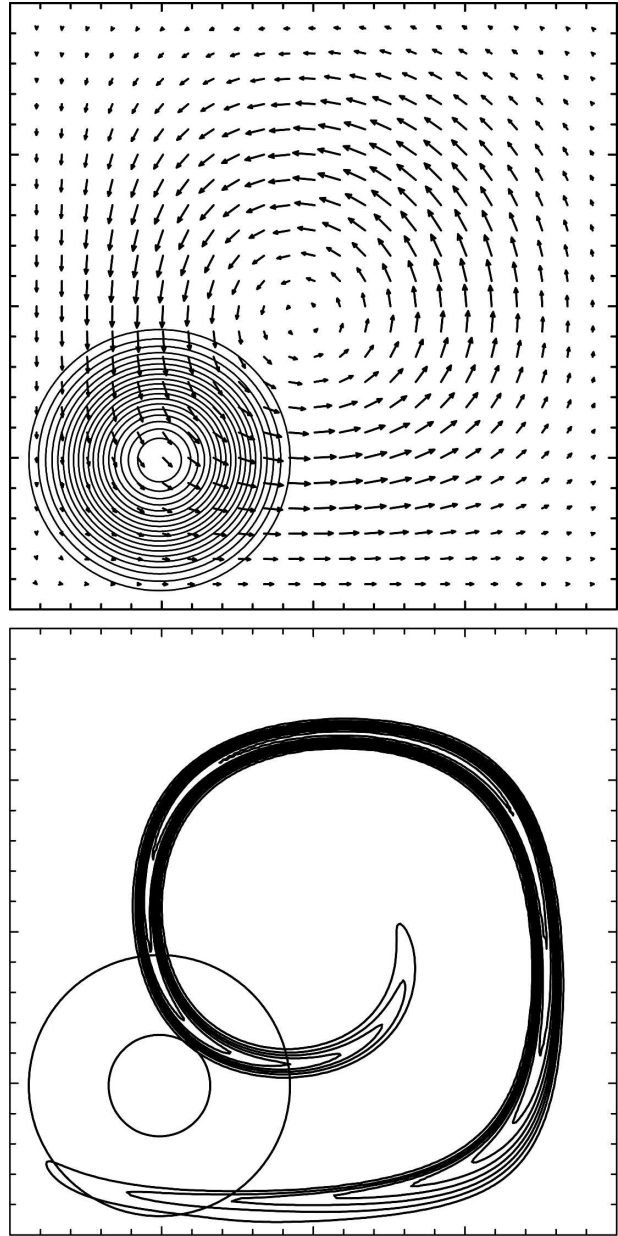


FIG. A1. Solution for 2D test problem at (top)  $t = 0$  and 5 and (bottom)  $t = 2.5$ . Plotted as in Fig. 1 except for the  $t = 2.5$  solution, which is contoured with an interval of 0.1.

that the initial state is contorted but, after a flow reversal at time  $T/2$ , returns to its initial state at time  $T$ . The initial tracer field differs from the 2D test in that a discontinuity is present in the initial state,

$$\begin{aligned} \phi(x, y, z, t = 0) &= 1 & x < \frac{1}{2}, \\ &= 0 & x \geq \frac{1}{2}. \end{aligned}$$

The velocity fields are given by

$$u(x, y, t) = 2 \sin^2(\pi x) \sin(2\pi y) \sin(2\pi z) \cos(\pi t/T)$$

$$v(x, y, t) = -\sin(2\pi x) \sin^2(\pi y) \sin(2\pi z) \cos(\pi t/T)$$

$$w(x, y, t) = -\sin(2\pi x) \sin(2\pi y) \sin^2(\pi z) \cos(\pi t/T).$$

Solutions at the midtime  $T/2$  and the end time  $T$  are given in Fig. 6 and are very similar to that presented in Leveque (1996, section 11.2).

### c. PPM advection scheme

The PPM scheme used herein is the nonmonotonized PPM advection described in Carpenter et al. (1990). PPM advection provides the fluxes  $f_{i+1/2}$  used to evaluate the flux divergence operator  $F_x$  in (4) or to compute the perturbation flux  $f'$  in (6), which, combined with the integer fluxes, are used in (4) in the Courant-number-unlimited formulation. Defining  $\phi_i$  as the control-volume average mixing ratio for cell  $i$ , zone edge values  $\hat{\phi}$  can be defined as

$$\hat{\phi}_{i+1/2} = [7(\phi_{i+1} + \phi_i) - (\phi_{i+2} + \phi_{i-1})]/12.$$

The flux through the  $i + 1/2$  face can be written as

$$f(\phi)_{i+1/2} = \rho u_{i+1/2} [\hat{\phi}_{i+1/2} - \text{Cr}(\hat{\phi}_{i+1/2} - \phi_i) - \text{Cr}(1 - \text{Cr})(\hat{\phi}_{i-1/2} - 2\phi_i + \hat{\phi}_{i+1/2})]$$

for  $\text{Cr} > 0$  and

$$f(\phi)_{i+1/2} = \rho u_{i+1/2} [\hat{\phi}_{i+1/2} + \text{Cr}(\hat{\phi}_{i+1/2} - \phi_{i+1}) + \text{Cr}(1 + \text{Cr})(\hat{\phi}_{i+1/2} - 2\phi_{i+1} + \hat{\phi}_{i+3/2})]$$

for  $\text{Cr} < 0$ . The Courant number  $\text{Cr} = (u_{i+1/2})\Delta t/\Delta x$ .

### REFERENCES

- Bermejo, R., and J. Conde, 2002: A conservative quasi-monotone semi-Lagrangian scheme. *Mon. Wea. Rev.*, **130**, 423–430.
- Carpenter, R. L., K. K. Droegemeier, P. R. Woodward, and C. E. Hane, 1990: Application of the Piecewise Parabolic Method (PPM) to meteorological modeling. *Mon. Wea. Rev.*, **118**, 586–612.
- Clappier, A., 1998: A correction method for use in multidimensional time-splitting advection algorithms: Application to two- and three-dimensional transport. *Mon. Wea. Rev.*, **126**, 232–242.
- Durran, D. R., 1999: *Numerical Methods for Wave Equations in Geophysical Fluid Dynamics*. 1st ed. Springer-Verlag, 465 pp.
- Easter, R. C., 1993: Two modified versions of Bott's positive definite numerical advection scheme. *Mon. Wea. Rev.*, **121**, 297–304.
- Leonard, B. P., 1991: The ULTIMATE conservative difference scheme applied to one-dimensional advection. *Comput. Meth. Appl. Mech. Eng.*, **88**, 17–74.
- , A. P. Lock, and M. K. MacVean, 1996: Conservative explicit unrestricted-time-step multidimensional constancy-preserving advection schemes. *Mon. Wea. Rev.*, **124**, 2588–2606.
- Leslie, L. M., and R. J. Purser, 1995: Three dimensional mass-conserving semi-Lagrangian schemes employing forward trajectories. *Mon. Wea. Rev.*, **123**, 2551–2566.
- Leveque, R. J., 1996: High-resolution conservative algorithms for advection in incompressible flow. *SIAM J. Numer. Anal.*, **33**, 627–665.
- Lin, S.-J., and R. B. Rood, 1996: Multidimensional flux-form semi-Lagrangian transport schemes. *Mon. Wea. Rev.*, **124**, 2046–2070.
- Nair, R. D., and B. Machenhauer, 2002: The mass-conservative cell-integrated semi-Lagrangian advection scheme on the sphere. *Mon. Wea. Rev.*, **130**, 649–667.
- Smolarkiewicz, P. K., 1989: Comment on "A positive definite advection scheme obtained by nonlinear renormalization of the advective fluxes." *Mon. Wea. Rev.*, **117**, 2626–2632.
- , and J. A. Pudykiewicz, 1992: A class of semi-Lagrangian approximations for fluids. *J. Atmos. Sci.*, **49**, 2082–2096.
- Staniforth, A., and J. Cote, 1991: Semi-Lagrangian integration schemes for atmospheric models: A review. *Mon. Wea. Rev.*, **119**, 2206–2223.
- Stevens, D. E., and C. Bretherton, 1996: A forward-in-time advection scheme and adaptive multilevel flow solver for nearly incompressible atmospheric flow. *J. Comput. Phys.*, **129**, 284–295.
- Strang, G., 1968: On the construction and composition of difference schemes. *SIAM J. Numer. Anal.*, **5**, 506–517.
- Thuburn, J., 1996: Multidimensional flux-limited advection schemes. *J. Comput. Phys.*, **123**, 74–83.
- Walcek, C. J., 2000: Minor flux adjustment near mixing ratio extremes for simplified yet highly accurate monotonic calculation of tracer advection. *J. Geophys. Res.*, **105**, 9335–9348.